Enhanced Densification of PM Steels by Liquid Phase Sintering with Boron-Containing Master Alloy

MAHESWARAN VATTUR SUNDARAM, KUMAR BABU SURREDDI, EDUARD HRYHA, ANGELA VEIGA, SIGURD BERG, FRANSISCO CASTRO, and LARS NYBORG

Reaching high density in PM steels is important for high-performance applications. In this study, liquid phase sintering of PM steels by adding gas-atomized Ni-Mn-B master alloy was investigated for enhancing the density levels of Fe- and Mo- prealloyed steel powder compacts. The results indicated that liquid formation occurs in two stages, beginning with the master alloy melting (LP-1) below and eutectic phase formation (LP-2) above 1373 K (1100 °C). Mo and C addition revealed a significant influence on the LP-2 temperatures and hence on the final densification behavior and mechanical properties. Microstructural embrittlement occurs with the formation of continuous boride networks along the grain boundaries, and its severity increases with carbon addition, especially for 2.5 wt pct of master alloy content. Sintering behavior, along with liquid generation, microstructural characteristics, and mechanical testing revealed that the reduced master alloy content from 2.5 to 1.5 wt pct (reaching overall boron content from 0.2 to 0.12 wt pct) was necessary for obtaining good ductility with better mechanical properties. Sintering with Ni-Mn-B master alloy enables the sintering activation by liquid phase formation in two stages to attain high density in PM steels suitable for high-performance applications.

DOI: 10.1007/s11661-017-4383-4

I. INTRODUCTION

POWDER metallurgy (PM) steels for high-performance applications are of significant interest because of their low costs, flexibility in alloy design, and high volume production. However, reaching high density is not viable through conventional pressing and sintering which limits the usage of PM steel components in high-performance and demanding applications. Hence, achieving high density is essential to obtain the demanding mechanical properties that will enable PM parts to serve as an alternative to conventionally manufactured parts. High densities can be achieved either through pressure-based or sintering-based techniques or by combining both.[1–4] Sintering with liquid phase forming additives activates the sintering and enhances the final densification through the liquid phase sintering mechanisms (LPS).[5,6] Elements with lower atomic number such as P, B, and C are well suited for activating sintering of iron-based powders due to the difference in electronic structure, phase composition, and grain boundary cohesion.[7] Lower amounts of such liquid-forming additives results in better densification by the liquid phase sintering (which is a dominant mechanism) than the surface energy activation.[5]

Boron addition significantly improves the density of the PM steels by forming a liquid with iron at ~1447 K (1174 °C) due to the eutectic reaction $\gamma Fe + Fe_2B \rightarrow L$.[8] Once the liquid forms, more iron will be dissolved in the liquid, which results in persistent liquid formation. In PM steels, boron is introduced either as elemental boron[7,9–14] or ferroboron,[15–20] or master alloy,[21–24] or compounds like hBN or B_4C.[25,26] Enhanced density levels were reached with elemental boron addition for both the carbonyl and water-atomized powders.[7] Ferroboron tends to agglomerate, resulting in inhomogeneous density distribution during sintering.[26] Selecká *et al.* [15] observed an increase in density by introducing ferroboron in Fe-Mo-prealloyed systems only when the boron content reaches beyond 0.2 wt pct. The design of master alloy is based on proper selection of alloy systems which can melt at lower melting temperatures so as to enable liquid phase sintering.[27] The elements such

MAHESWARAN VATTUR SUNDARAM, EDUARD HRYHA, and LARS NYBORG are with the Department of Industrial and Materials Science, Chalmers University of Technology, 412 96 Gothenburg, Sweden. Contact e-mail: vattur@chalmers.se KUMAR BABU SURREDDI is with the Materials Science, Dalarna University, 791 88 Falun, Sweden. ANGELA VEIGA and FRANSISCO CASTRO are with the CEIT, Paseo de Manuel Lardizábal 15, 20018, San Sebastián, Spain. SIGURD BERG is with the Höganäs AB, 263 83 Höganäs, Sweden.
Manuscript submitted June 10, 2017.

Published online: 24 October 2017

as Mn, Si, Cr, Ni can also be introduced without affecting the base powder compressibility.[28] When boron is introduced in the master alloy, it provides the flexibility of generating a liquid phase from the melting of the master alloy and the eutectic reaction between iron and boron.

In this present study, liquid phase generation was assessed during sintering for pure iron and Fe-Mo-prealloyed powder compacts admixed with gas-atomized Ni-Mn-B master alloy (MA) powder. The densification behavior during sintering and microstructure of the PM compacts were studied. Furthermore, the effect of alloying elements, *i.e.*, carbon and molybdenum, MA content (2.5 and 1.5 wt pct) on the densification behavior was analyzed. Thermodynamic simulations using Thermo-Calc were carried out to predict the amount of liquid phase and its formation temperature so as to correlate with the experimental observations. The mechanical properties of the PM compacts were also analyzed to identify the applicability of these materials for high-performance applications.

II. MATERIALS AND METHODS

In this study, the water-atomized iron powder (ASC100.29) and Fe-Mo-prealloyed powder (X-Astaloy 0.45Mo) from Höganäs AB were used as the base powder. Gas-atomized Ni-Mn-B master alloy (MA) powder, known as CEITALOY HD, developed by CEIT, Spain[22,29] with the nominal composition of 46 wt pct Mn, 46 wt pct Ni, and 8 wt pct B was used. The MA powder was produced by Höganäs AB using gas atomization and sieved below 45 μm. The MA powder was admixed with the base iron powders along with 0.4 wt pct Kenolube lubricant. The powder mixes were uniaxially pressed to impact bars with dimensions ($10 \times 10 \times 55$ mm^3) according to ISO 5754 to reach ~7.3 g cm^{-3} density. The influence of carbon was studied by admixing 0.3 wt pct of natural graphite (UF4 from Kropfmühl). The master alloy addition of 2.5 and 1.5 wt pct was studied, which leads to an overall boron content of 0.2 and 0.12 wt pct, respectively. Higher MA addition was studied initially and then MA content was optimized to improve the mechanical properties of the components. Table I shows a summary of all the combination of powder mixtures and the designation that will be used henceforth. The six samples were chosen to study the influence of carbon, molybdenum, and MA content on densification behavior and mechanical properties.

All the samples were de-lubricated in a laboratory tube furnace at 723 K (450 °C) for 30 minutes under pure N_2 atmosphere. DSC was performed on de-lubricated samples with a heating and cooling rate of 10 K/min in high-purity argon (99.9999 pct) to study heat and phase changes. Simultaneous TG/DTA/DSC thermal analyzer STA 449 F1 Jupiter® from Netzsch was used for DSC measurements. All the laboratory sintering experiments were performed in a Netzsch 402L push rod dilatometer to detect the dimensional changes associated with sintering. Sintering was performed at 1513 K (1240 °C) for 30 minutes in Ar-50H_2 atmosphere with the heating and cooling rate of 10 and 30 K/min, respectively. In order to detect the formation and distribution of liquid phase during the heating stage as well as its effect on microstructure formation, interrupted sintering trails were performed at temperatures of 1273 K, 1373 K, and 1513 K (1000 °C, 1100 °C, and 1240 °C) for 1 minute with the same heating and cooling rates as above. All sintered samples were tempered in air at 473 K (200 °C) and then impact tested. Density measurements were performed by measuring the dimensions and sample mass for green compacts and by Archimedes' principle according to ISO 3369 for sintered samples. For metallographic investigations, the samples were grounded, polished, and then etched using 3 pct nital. A Leica DMRX optical microscope was used for microstructural investigation. LEO 1550 Gemini scanning electron microscopy (SEM) combined with energy dispersive X-ray analysis (EDX, X-Max, Oxford Instruments) was used for microscopy study. The fractography study was performed on the fracture surfaces obtained after impact testing using SEM. Hardness was measured using Wolpert Dia Tester with Vickers scale of 10 kgf (HV10). Thermo-Calc software using TCFE8 database, based on the CALPHAD method,[30] was used to identify temperature and the volume fraction of liquid phase formed under equilibrium conditions.

III. RESULTS

A. *Analysis of Liquid Phase Sintering from Dilatometry Curves*

Figure 1(a) shows the curves obtained from dilatometry, with time along the *X*-axis and dilatation (dL/L_o) as well as temperature along the *Y*-axis for the two samples: one is the PM compact with boron-containing master alloy (Fe + 2.5MA + C) and another one is the

Table I. Composition of the PM Samples (All Values are in Weight Percent)

Mixture Designation	Mo	C	MA	Fe
Fe + 2.5MA	—	—	2.5	bal.
Fe + 2.5MA + C	—	0.3	2.5	bal.
Fe-Mo + 2.5MA	0.45	—	2.5	bal.
Fe-Mo + 2.5MA + C	0.45	0.3	2.5	bal.
Fe-Mo + 1.5MA	0.45	—	1.5	bal.
Fe-Mo + 1.5MA + C	0.45	0.3	1.5	bal.

PM compact without master alloy addition (Fe + C), sintered at 1513 K (1240 °C) for 30 minutes. In Figure 1(a), 1-2 represents a heating stage, 2-3 dwell or sintering stage, and 3-4 is the cooling stage. Sintering of PM compact with boron-containing master alloy (Fe + 2.5MA + C) clearly exhibits strong shrinkage as compared to the reference PM compact (Fe + C), see Figure 1(a). Figures 1(b) through (d) show the dilatometric curves with temperature along *X*-axis and dilatation as well as dilatation rate (dL/dt) along the *Y*-axis for various samples. Figure 1(b) shows the dilatometric and dL/dt curves during the heating stage for Fe + 2.5MA + C and Fe + 2.5MA in order to distinguish the difference in the dilation of the samples containing boron-based master alloy with and without carbon addition. Figures 1(c) and (d) show the dilatometric curves of Fe-Mo + 2.5MA and Fe-Mo + 1.5MA samples with and without carbon addition. Table II shows the analyzed data from the dilatometry sintering curves as seen in Figures 1(b) through (d).

Observations from the dilatometry curves for Fe + 2.5MA, Fe-Mo + 2.5MA, and Fe-Mo + 1.5MA without carbon show that α-γ iron transition start and end temperatures are higher than for carbon-containing samples. After the α-γ transition, there is a continuous linear expansion until the samples reach the maximum expansion (peak) as indicated with the LP-1 segment in Figures 1(b) through (d). The shrinkage that begins right after the peak temperature continues throughout the sintering cycle as well as during cooling cycle. The overall shrinkage values, as shown in Table II, indicate that the major influence is from the amount of master alloy and carbon addition. The Fe-Mo + 2.5MA sample shows higher linear shrinkage compared to the Fe-Mo + 1.5MA and Fe + 2.5MA samples. The Fe + 2.5MA + C sample shows the initiation of shrinkage before reaching 1513 K (1240 °C), indicating that the formation of the liquid phase is well below the sintering temperature. Figure 1(b) clearly shows that the liquid formation occurs in two stages (boxes in the figure), the first stage (LP-1) and the second stage (LP-2). The LP-1 stage shows the shrinkage which is associated with the liquid phase formation due to the master alloy melting well below 1373 K (1100 °C), which spreads rapidly due to capillary action and excellent particle wetting resulting in shrinkage above 1373 K (1100 °C).

The LP-1 temperature in Table II is taken from the onset of the shrinkage portion in the dilatometry curve. A continuous shrinkage is observed from the dL/L_o curve till the final cooling. However, analysis of the dL/dt curve during shrinkage stage clearly shows a wide peak with multiple slopes in all the samples containing master alloys, indicating that secondary densification processes. The initial portion of the dL/dt curve exhibits a rapid downward slope which can be correlated to the rapid shrinkage associated from the master alloy melting which enables the initial densification, and the later part of the curve shows a deviation in the slope with a sudden deflection with a positive slope. This can be related to the formation of the secondary liquid phase from the eutectic reaction.

The shrinkage, *i.e.,* LP-1 stage, begins at a lower temperature in carbon-containing samples as compared to carbon-free samples. Shrinkage also starts earlier for Mo-containing samples, see Table II. The dL/dt curve

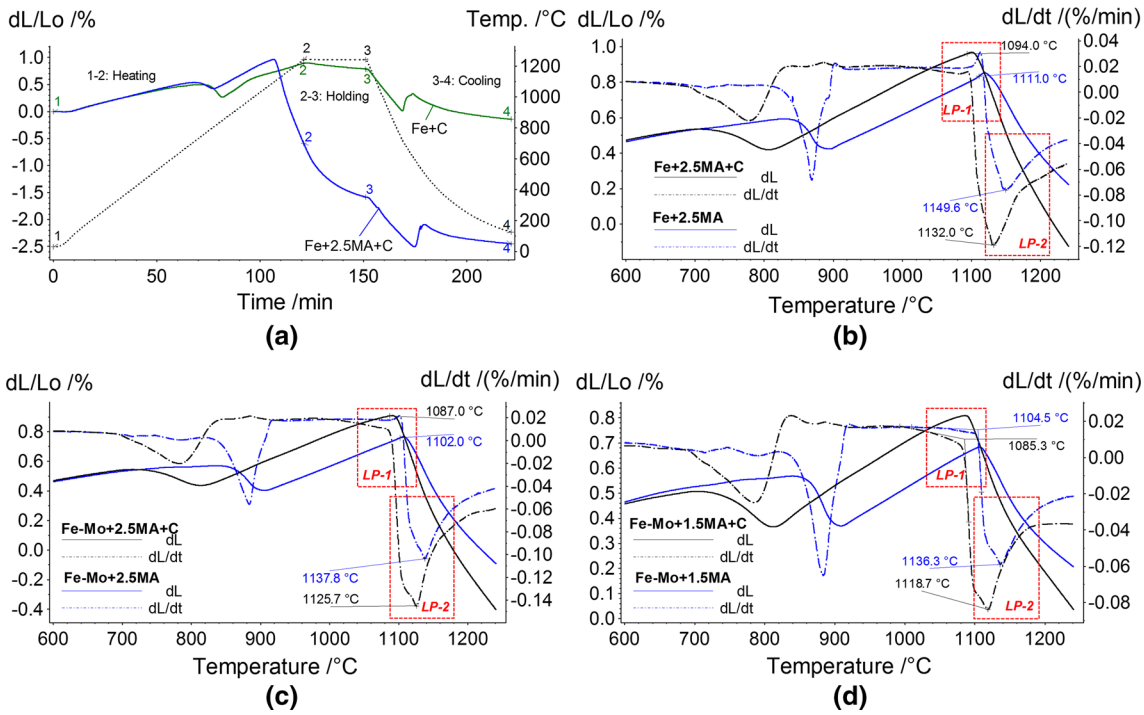

Fig. 1—Dilatometry curves of Fe + C with master alloy and without master alloy (*a*), Fe + 2.5MA with and without carbon (*b*), Fe-Mo + 2.5MA with and without carbon (*c*), and Fe-Mo + 1.5MA with and without carbon (*d*).

Table II. Analysis from Dilatometry Curves of the PM Samples

	Temperature, K (°C)		Dimensional Change (dL/L_o) (pct)		
Material	Peak LP-1	dL/dt LP-2	From Peak Till Sintering	2-3: Holding	Total
Fe + 2.5MA	1384 (1111)	1423 (1150)	−0.6	−0.7	−1.4
Fe + 2.5MA + C	1367 (1094)	1405 (1132)	−1.1	−0.7	−2.0
Fe-Mo + 2.5MA	1375 (1102)	1411 (1138)	−0.9	−0.7	−1.8
Fe-Mo + 2.5MA + C	1360 (1087)	1399 (1126)	−1.3	−0.7	−2.1
Fe-Mo + 1.5MA	1379 (1106)	1409 (1136)	−0.5	−0.5	−1.3
Fe-Mo + 1.5MA + C	1359 (1086)	1392 (1119)	−0.8	−0.6	−1.4

shows a sharp increase in the shrinkage rate, reaching a maximum value for carbon-containing samples in the range between ~1393 K and ~1403 K (1120 °C to 1130 °C) and at about 20 K higher for the carbon-free materials. It is important to note the deviation of the peak in the case of dL/dt curve, indicating two overlapping processes of densification, most probably related to the generation of the second liquid phase. It can be seen from Table II that the shrinkage obtained after ~1373 K (1100 °C) until the sintering temperature of 1513 K (1240 °C) is greatest for the Fe-Mo + 2.5-MA + C sample, containing the highest amount of boron and carbon. Hence, it corroborates to the shrinkage in this region and is associated with the amount of the liquid generated from the master alloy melting and from further eutectic reaction with iron. The shrinkage during sintering-holding is similar for all the samples admixed with 2.5 MA and is slightly lower for the 1.5 MA samples. The overall shrinkage is significantly influenced by alloying elements Mo, C, and the amount of MA addition.

B. *Eutectic Liquid Formation (LP-2) Analysis from DSC Curves*

Figure 2 shows the DSC curves for all six samples. Invariably, all samples reveal the curie temperature of around 1046 K (773 °C) during the heating stage. A clear transition peak from $\alpha \rightarrow \gamma$ is observed around 1185 K (912 °C) for the samples without carbon addition. Also, the effect of Mo as a ferrite stabilizer is clear from the slight shift in the $\alpha \rightarrow \gamma$ transformation to a higher temperature. The peak from master alloy melting, that is around 1292 K (1019 °C) for the MA powder,[29] is not observed due to the low master alloy content. The endothermic peak is observed at a higher temperature, between 1373 K and 1473 K (1100 °C and 1200 °C) for all the samples. This results in the liquid phase formation and can be correlated to the second stage of densification due to eutectic liquid generation, marked as an LP-2 stage from the dilatometry curves and DSC peaks, see Figures 1 and 2. The presence of Mo shifts the LP-2 onset slightly to lower temperature by ~10 K and ~20 K with the addition of carbon see Table III. In the case of an Fe-based system, adding carbon reduces onset temperature by ~10 K. From analyzing the onset and end points of DSC peak from Figure 2, it is evident that the alloying elements Mo and C have a significant influence on the eutectic liquid formation temperature.

C. *Estimation of Eutectic Liquid Formation (LP-2) from Simulations*

Reaching higher density is correlated to the volume fraction of liquid phase generated through both master alloy melting and eutectic formation. Using Thermo-Calc with TCFE8 database, simulations were performed to predict the equilibrium phases formed at different temperatures as well as the amount of the eutectic liquid phase. This can be correlated further to the liquid phase formation during sintering. The predicted molar volume fraction of liquid at the sintering temperature of 1513 K (1240 °C) is presented in Table IV. Figure 3(a) shows the comparison between onset eutectic temperatures estimated from DSC experiments and Thermo-Calc simulations.

For Mo-containing samples, Thermo-Calc predicts a shift in onset temperature to a slightly higher temperature, see Figure 3(a), resulting in more liquid molar volume at the sintering temperature, see Figure 3(b). The carbon addition clearly lowers the onset temperature significantly in all cases to ~30 K and contributes to higher molar volume fraction of liquid, see Figure 3(b). The molar volume fraction of liquid formed at the sintering temperature is increased by ~1.1 vol pct for 1.5 MA with and without carbon, whereas for 2.5 MA with and without carbon the increase in LP is ~1.75 vol pct from the onset. Both carbon and molybdenum accelerate sintering by promoting the formation of liquid at a much lower temperature. Simulations showed a delay in LP-2 formation, as seen in Figure 3(b), for Mo-containing systems, and the total molar volume fraction of liquid after sintering in the case of Mo-prealloyed systems is larger than in the case of pure Fe.

D. *Microstructure and Properties*

Figure 4 shows the optical micrographs of the samples sintered in the dilatometer at 1273 K and 1373 K (1000 °C and 1100 °C) for 1 minute and of samples sintered at 1513 K (1240 °C) for 30 minutes. The different stages of the liquid phase sintering can be clearly observed in the optical micrographs. Until the temperature of 1273 K (1000 °C), only initial stage of

the master alloy melting is evident, see Figure 4, that is in accordance with the DSC of the MA powder.[29] The micrographs of the samples at 1273 K (1000 °C) show the pore formation inside MA particles in connection to the partial melting of the master alloy particles; however, overall MA particle was not completely melted. It can also be observed that there is no spreading of this liquid through the particle boundaries. Liquid phase along the particle and grain boundaries is seen after sintering at 1373 K (1100 °C) Figures 4 (b) and (e). The optical micrographs show the presence of the spherical pore in the sites of former MA-particle location as well as the spreading of the liquid phase along the particles and grain boundaries. This is in good agreement with the beginning of shrinkage stage associated with the liquid phase formation as shown in LP-1 in Figure 1 and Table II.

The secondary (LP-2) liquid formation occurs once eutectic reaction begins, which accelerates the shrinkage further until sintering as seen from the dilatometry curves, see Figure 1, and results in a typical eutectic microstructure as seen from optical micrographs of the samples sintered at 1513 K (1240 °C). Hence, the optical micrographs in Figure 4 show a typical characteristic behavior of the liquid phase sintering through the formation of the liquid phase and following the liquid spreading and the rearrangement in this case with two distinct melting regimes, LP-1 and LP-2.

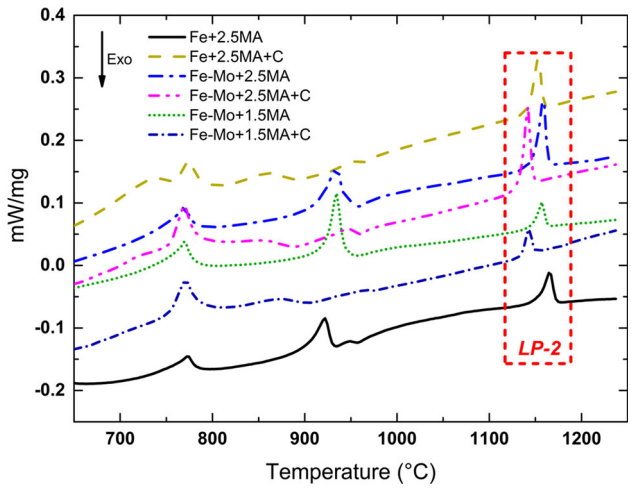

Fig. 2—DSC curves of the compacts during heating stage revealing multiple peaks.

Table V shows the results of the density, hardness, and impact energy values of the samples sintered at 1513 K (1240 °C) for 30 minutes. The impact energy (IE) values significantly decreased from 82 to 24 J with carbon addition, whereas the density and hardness increased for Fe + 2.5MA + C as compared to Fe + 2.5MA. The presence of Mo also shows a drastic decrease in impact energy, but also enhanced density and hardness values, when changing from Fe + 2.5MA to Fe-Mo + 2.5MA and from Fe + 2.5MA + C to Fe-Mo + 2.5MA + C. Addition of molybdenum strengthen the matrix, as observed from increased hardness values, but the impact energy values drops due to the microstructural embrittlement. In addition, when carbon is added, these effects are more pronounced and decrease the impact energy but increase the hardness and density. It is clearly seen from Table IV that with increasing MA content and addition of C and Mo, a higher volume fraction of liquid is formed that contributes significantly to densification. The impact energy values drastically decrease with the addition of Mo and C due to embrittlement. When the MA content is reduced from 2.5 to 1.5 wt pct, impact energy is improved for 1.5 wt pct MA samples with and without carbon as compared to 2.5 wt pct MA samples.

The fracture surface of the samples after sintering at 1513 K (1240 °C) for 30 minutes reveals well-sintered microstructures and displays predominantly transparticle cleavage failure, see Figures 5(a), (b), and (d). In case of Fe-Mo + 1.5MA, the failure is a mixture of transparticle cleavage and ductile failure with large dimples initiated by secondary phases of pores shown as magnified insets in Figure 5(c) in red. Samples with carbon, Figures 5(b) and (d), show brittle failure with predominantly transgranular cleavage fracture, and the

Table IV. Liquid Volume Fraction at 1513 K (1240 °C) from Thermo-Calc

Material	Molar Volume Fraction (pct)
Fe + 2.5MA	5.9
Fe + 2.5MA + C	7.2
Fe-Mo + 2.5MA	6.0
Fe-Mo + 2.5MA + C	7.4
Fe-Mo + 1.5MA	3.3
Fe-Mo + 1.5MA + C	4.1

Table III. Eutectic Onset and End Temperatures from DSC Curves in Fig. 2

	Temperature, K (°C)		
Material	Onset	End	ΔT
Fe + 2.5MA	1427 (1154)	1445 (1172)	18
Fe + 2.5MA + C	1416 (1143)	1432 (1159)	16
Fe-Mo + 2.5MA	1422 (1149)	1436 (1163)	14
Fe-Mo + 2.5MA + C	1407 (1134)	1420 (1147)	13
Fe-Mo + 1.5MA	1420 (1147)	1435 (1162)	15
Fe-Mo + 1.5MA + C	1409 (1136)	1422 (1149)	13

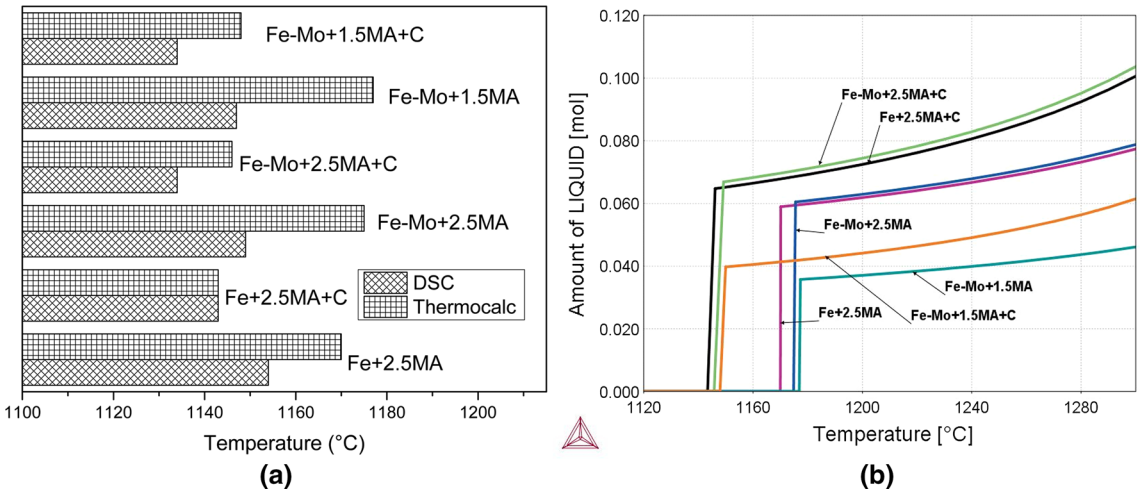

Fig. 3—Onset eutectic temperatures estimated from the experimental data and simulation (*a*); amount of liquid phase estimated using Thermo-Calc from the equilibrium phases (*b*).

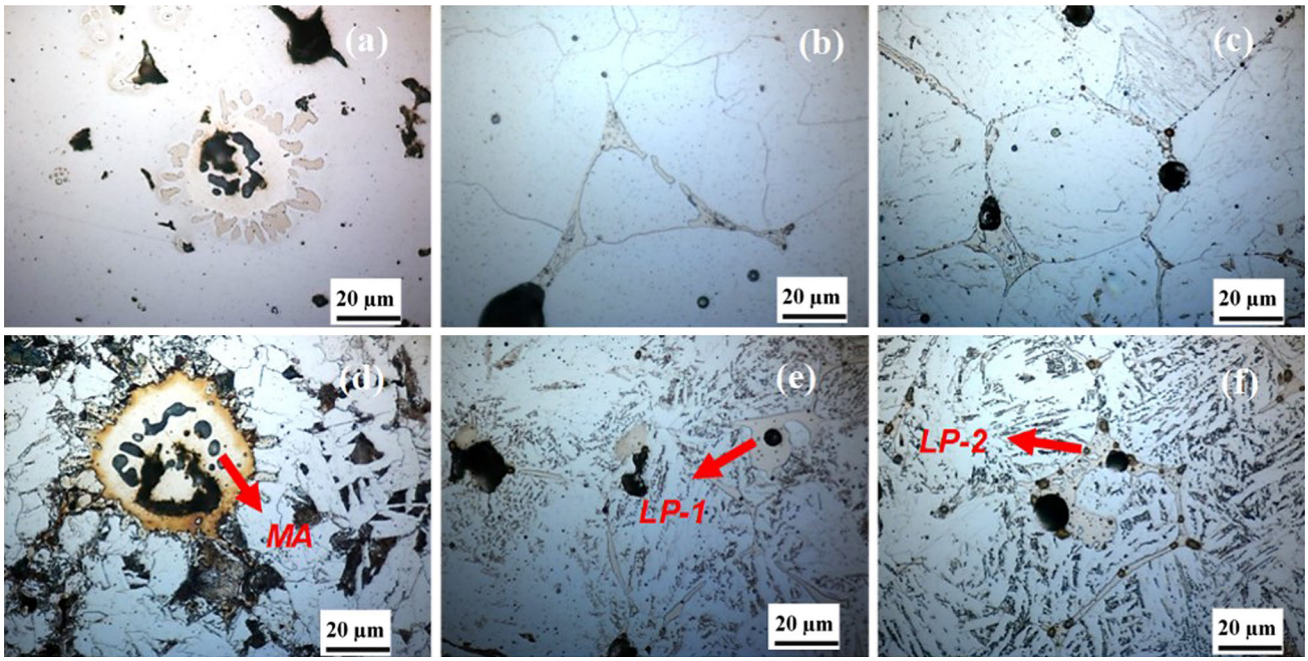

Fig. 4—Optical micrographs of Fe-Mo + 2.5MA (*a*) through (*c*) and Fe-Mo + 2.5MA + C (*d*) through (*f*) at different sintering temperatures 1273 K (1000 °C)—1 min (a, d), 1373 K (1100 °C)—1 min (b, c), and 1513 K (1240 °C)—30 min (c, f).

Table V. Density, Impact Energy, and Hardness Results of all the Samples Sintered at 1513 K (1240 °C) for 30 Min in Ar-50H_2 (*SD* Sintered Density, *IE* Impact Energy)

Material	SD(g/cm^3)	IE (J)	Hardness HV10
Fe + 2.5MA	7.48	82	110 ± 5
Fe + 2.5MA + C	7.63	24	190 ± 3
Fe-Mo + 2.5MA	7.58	26	187 ± 5
Fe-Mo + 2.5MA + C	7.67	13	240 ± 6
Fe-Mo + 1.5MA	7.49	121	161 ± 17
Fe-Mo + 1.5MA + C	7.55	49	231 ± 10

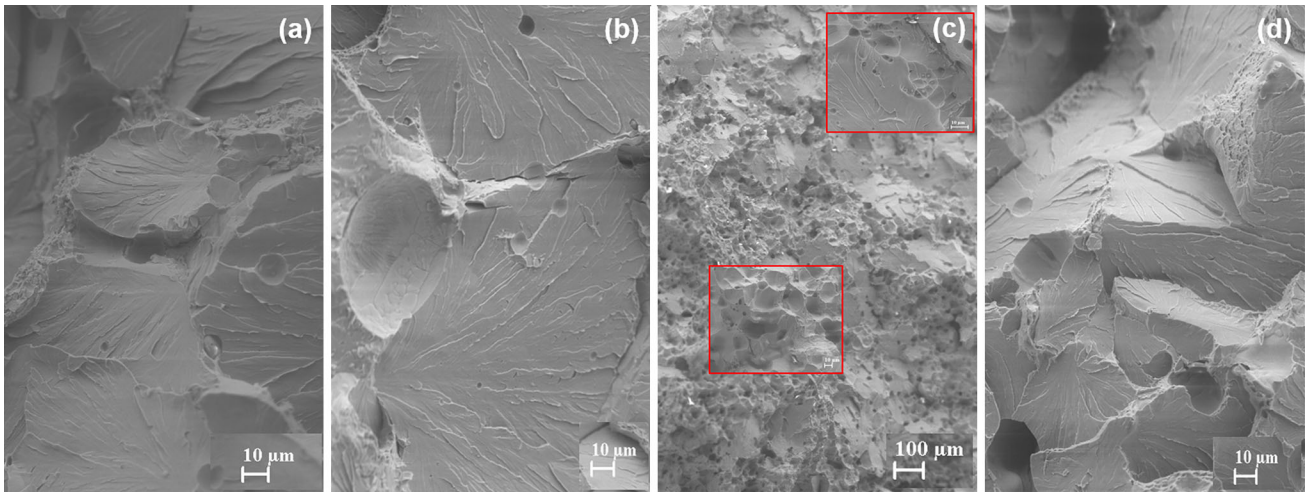

Fig. 5—Fractography of the samples sintered at 1513 K (1240 °C)—30 min after impact testing, Fe-Mo + 2.5MA (*a*), Fe-Mo + 2.5MA + C (*b*), Fe-Mo + 1.5MA (*c*), and Fe-Mo + 1.5MA + C (*d*).

Fe-Mo + 1.5MA showing some regions of ductile dimple failure.

IV. DISCUSSION

The addition of boron-containing master alloy to iron and iron-molybdenum PM compacts reveals significant shrinkage during sintering above 1373 K (1100 °C). The sintering process and densification are activated due to the liquid phase formation. Sintering follows the mechanisms of liquid phase sintering,[5] starting from melting, spreading, rearrangement, and shrinkage. The results from the dilatometry, DSC, and microstructural study show two regimes of liquid phase formation: LP-1 and LP-2. The formation of initial liquid phase LP-1 is due to melting of the master alloy ~1292 K (1019 °C) from DSC analysis[29] and is in the same range as the liquidus temperature for the Ni-Mn binary system ~1293 K (1020 °C)[31] and the eutectic temperature of the Ni-B binary system ~1291 K (1018 °C).[32] The dilatometry curves from Figures 1(b) through (d) indicate that the shrinkage rate is rapid above ~1373 K (1100 °C). This is due to the initial rearrangement of the powder particles from the prior master alloy melting (LP-1). After that, the eutectic formation occurs (LP-2) as evident from the endothermic peaks of DSC, see Figure 2. This is also shown by Thermo-Calc simulations having similar liquid formation temperature, see Figure 3(a). Also, the LP-2 stage as indicated by the dL/dt of the dilatometry curves in Figures 1(b) through (d) can be related to the initiation of the eutectic melting, where the shrinkage rate starts to deviate.

This melting behavior is enormously effected by the presence of Fe and Fe-Mo as it depends on the thermodynamic stability of the boride phases formed with Ni and Mn. Mo in Fe is homogenously distributed within the iron powders as it is prealloyed, and the presence of B from master alloy favors the formation of molybdenum borides since the free energy of Mo_2B and MoB_2 is much lower than the corresponding Fe borides.[17] For both Fe and Fe-Mo systems, the eutectic formation occurs with the following reaction: $\gamma Fe + Fe_2B \rightarrow L$, and $\gamma(Fe, Mo) + (Fe, Mo)_2B \rightarrow L$. This eutectic formation will dissolve more Fe and generates more liquid phase resulting in the accommodation of grains, pore elimination, and grain coarsening. Sarasola *et al.* have reported that increase in the Mo content up to 3.5 wt pct suppressed the liquid formation, as all the B in the system is expended by Mo to form borides.[14] Hence, having a lower Mo/B ratio is an advantage as less Mo will be available to form borides. For Fe-Mo + 2.5MA and Fe-Mo + 1.5MA with and without carbon, the shrinkage initiation is at a similar temperature; however, the shrinkage is significantly larger for Fe-Mo + 2.5MA as observed from the dilatometry curves, see Figures 1(c) and (d). From Tables II and III, the experimental results of the dilatometry curves and DSC traces, it is evident that Mo addition shifts the liquid formation stages LP-1 and LP-2 to lower temperatures, but the simulations from Thermo-Calc, see Figure 3(b), showed a higher LP-2 formation temperature. However, both experiments and simulations agree that Mo presence contributes to the formation of a higher amount of liquid volume fraction, see Table IV, but the delay in formation of LP-2 temperature from the predicted simulations is due to the equilibrium conditions.[9] Results clearly show that the amount of liquid phase and the melting temperatures are slightly lower as simulated by Thermo-Calc and this is related to some inaccuracy of the thermodynamic data for the system. In addition, during simulations in Thermo-Calc, a homogeneous system is assumed, which is not the case for the Fe-MA powder system, characterized by large concentration gradients between the sites of MA location and core of the base iron/steel particles.

Along with prealloyed Mo, carbon also has a significant effect on the densification which is evident from Figure 6 for the samples with and without carbon. Its effect is more pronounced when sintered above 1373 K (1100 °C), that is, during the second stage of the liquid formation (LP-2). Both the DSC results and

Thermo-Calc simulations from Figure 3(a) show that the carbon presence lowers the LP-2 formation temperature as observed elsewhere.[9,21] This also results in higher liquid molar volume fraction at 1513 K (1240 °C) as indicated in Table IV, which enhances the density levels. Also, increasing master alloy from 1.5 to 2.5 wt pct facilitates the formation of more liquid volume fraction which results in an increase in densification from 2 to 5 pct depending on the amount of carbon content. Introducing boron as a master alloy has a significant impact on the densification, as observed from this study

I. Both the LP-1 (shrinkage from master alloy melting) and LP-2 eutectic liquid formation temperatures are strongly influenced by the presence of C and slightly of Mo, with both shifting the liquid formation to lower temperatures.
II. The amount of liquid formation is increased with the presence of Mo, C, and the amount of MA content, which is evident from the enhanced density levels.

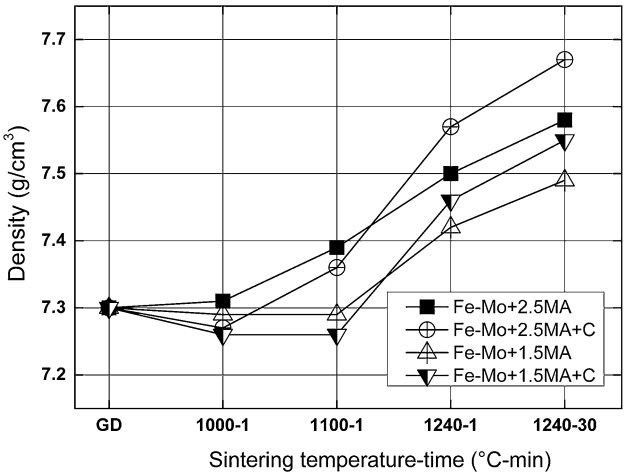

Fig. 6—Sintered density plot for Mo-prealloyed samples after interrupted sintering trails showing increasing density levels after sintering at 1373 K (1100 °C) for 1 min.

Ni addition accelerates the boron diffusion in the γ-iron, similar to the carbon behavior in the presence of Ni[33,34] and increases the density of the PM steels.[15,35] Liu *et al.*[36] have shown near-full density after sintering pure iron with 1 wt pct Ni and 0.3 wt pct B. As indicated by Wu *et al.*,[37] the eutectic structure consists primarily of M_2B or $M_3(B,C)$ with Fe, Mo, and Mn being the main elements with the presence of carbon and boron and Ni is absent from the eutectic structures as it will be distributed in the iron matrix. This can also be observed from the EDX analysis of the boride network as shown in Figure 7(b). The presence of Mn does not show much influence overall but is observed along with Fe in the boride network.

Sintering with boron addition forms eutectic phase as a continuous layer along the grain boundaries, especially for 2.5 MA samples (0.2 wt pct boron), even though adding more boron and carbon increases the volume fraction of liquid which eventually increases the density but not necessarily the mechanical properties as it results in embrittlement. The eutectic phases along the grain boundaries are extremely hard, which eventually results in the inferior mechanical properties see IE values in Table V and have brittle failure see Figure 5. However, the 1.5 wt pct master alloy addition (0.12 wt pct of boron) gives enhanced ductility with the impact energy (IE) values greater than 100 J (see Table V), which is similar to the case of Fe-0.1B.[19] This is due to the formation of a discontinuous eutectic network along the grain boundaries as seen from Figure 7(a), where the borides formed are evident from Figure 7(b). Hence, the design of this alloy system is to avoid the formation of continuous boride network and to substitute discontinuous boride networks along the grain boundaries, as seen from Figures 7(a) and (b). In this way, intergranular embrittlement can be fully avoided, as observed in the case of stainless steel based PM systems where fully dense and ductile components with elongation as high as ~ 34 pct are obtained for 316 L.[23]

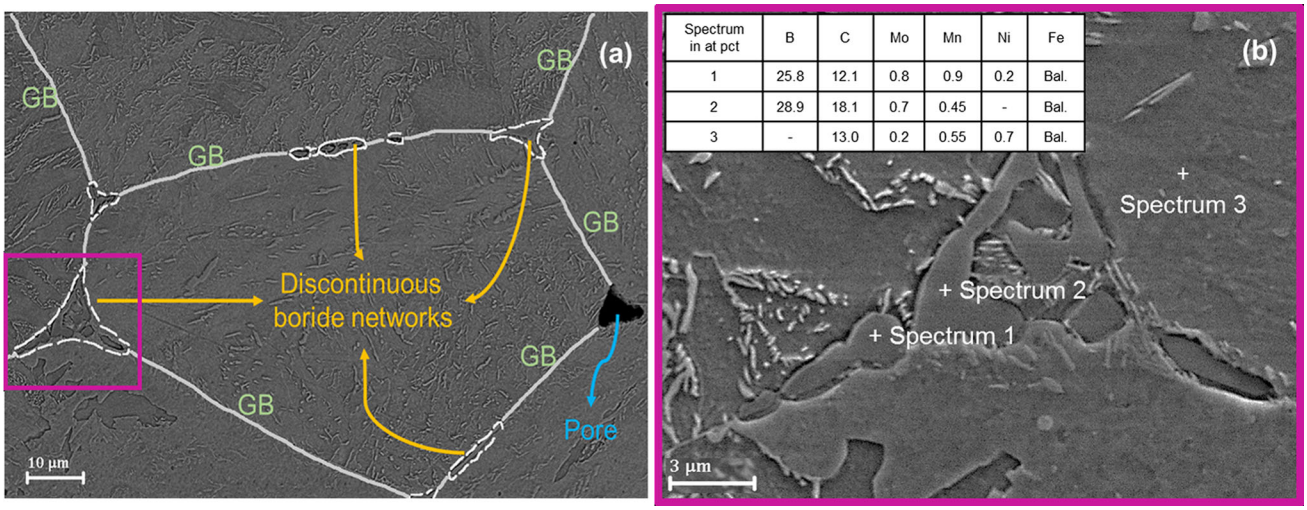

Fig. 7—SEM micrograph of Fe-Mo + 1.5MA + C sample with discontinuous eutectic boride networks along the grain boundary (*a*) and magnified micrograph of the eutectic structure indicating the boride presence from EDX analysis (*b*).

V. CONCLUSION

In this study, the liquid phase sintering of PM compacts with master alloy containing boron (Ni-Mn-B) added to water-atomized Fe and Fe-Mo-prealloyed base powders was investigated. Analysis of the densification behavior and identification of the liquid-forming stages during sintering through dilatometry and DSC analysis were performed. Carbon addition and MA alloy content were varied to observe their effect on the liquid formation temperature, properties, and performance.

1. The results obtained clearly indicate that the master alloy addition effectively enhances the density by ~2 to 4 pct through liquid phase formation during sintering.
2. Liquid phase formation occurs in two stages around 1273 K (1000 °C), first from the master alloy melting (LP-1) and second from the eutectic formation (LP-2).
3. Prealloyed Mo and C addition as admixed graphite shifts the liquid formation temperature to lower temperatures, especially the eutectic liquid formation.
4. This early shifting also contributes to the higher liquid volume fraction resulting in better densification.
5. Addition of carbon along with 2.5 wt pct MA content enables more liquid phase formation, and therefore there is a formation of interconnected boride network that results in embrittlement.
6. Reducing the MA content from 2.5 to 1.5 wt pct (to reach overall boron content from 0.2 to 0.12 wt pct) is necessary for improved mechanical properties in order to form a discontinuous boride network.

Boron control is essential to reach the sufficient densification and optimum mechanical properties which are suitable for the high-performance applications without compromising the dimensional stability of the PM components.

ACKNOWLEDGMENTS

The authors would like to acknowledge Vinnova (Swedish Agency for Innovation Systems) for funding the HIPERSINT project (Dnr: 2010-01619). Höganäs AB, Sweden, and CEIT (Centre for Technical Research and Studies), Spain are greatly acknowledged for their collaborations and contributions to the project.

OPEN ACCESS

REFERENCES

1. W.B. James: *Int. J. Powder Metall. Powder Technol.*, 1985, vol. 21, pp. 163–82.
2. U. Engström, C. Lindberg, and J. Tengzelius: *Powder Metall.*, 1992, vol. 35, pp. 67–73.
3. H.G. Rutz and F.G. Hanejko: *Adv. Powder Metall. Part. Mater.*, 1994, vol. 5, p. 117.
4. W.B. James: *Int. J. Powder Metall.*, 2005, vol. 41, pp. 31–36.
5. R.M. German: *Liquid Phase Sintering*, Springer Science & Business Media, Berlin, 1985.
6. B.A. James: *Powder Metall.*, 1985, vol. 28, pp. 121–30.
7. D.S. Madan and R.M. German: *Mod. Dev. Powder Metall.*, 1984, vol. 15, pp. 441–54.
8. P.K. Liao and K.E. Spear: *ASM Handbook*, ASM International, Ohio, 1992, vol. 3, pp. 2.8–9.8.
9. M.W. Wu: *Metall. Mater. Trans. A*, 2014, vol. 46A, pp. 467–75.
10. A. Molinari, T. Pieczonka, J. Kazior, S. Gialanella, and G. Straffelini: *Metall. Mater. Trans. A*, 2000, vol. 31A, pp. 1497–1506.
11. M. Sarasola, T. Gómez-Acebo, and F. Castro: *Powder Metall.*, 2005, vol. 48, pp. 59–67.
12. J. Karwan-Baczewska and M. Rosso: *Powder Metall.*, 2001, vol. 44, pp. 221–27.
13. J. Klein: *Preliminary Investigation of Liquid Phase Sintering in Ferrous Systems, California Univ., Berkeley (USA)*, Lawrence Berkeley Lab, Berkeley, 1975.
14. M. Sarasola, T. Gómez-Acebo, and F. Castro: *Acta Mater.*, 2004, vol. 52, pp. 4615–22.
15. M. Selecká, A. Šalak, and H. Danninger: *J. Mater. Process. Technol.*, 2003, vol. 143, pp. 910–15.
16. M. Momeni, C. Gierl, H. Danninger, and A. Avakemian: *Powder Metall.*, 2012, vol. 55, pp. 54–64.
17. E. Dudrova, M. Selecka, R. Bures, and M. Kabátová: *ISIJ Int.*, 1997, vol. 37, pp. 59–64.
18. D. Krecar, V. Vassileva, H. Danninger, and H. Hutter: *Anal. Bioanal. Chem.*, 2004, vol. 379, pp. 605–09.
19. V Vassileva, H Danninger, S Strobl, and C Gierl: Euro PM2007. 2007, 1: 53–58.
20. M. Marucci, A. Lawley, R. Causton, and S. Saritas: *Proc. Powder Metall. Congr. Exhib.* Orlando, Florida, USA, 2002.
21. Z. Xiu, A. Salwén, X. Qin, F. He, and X. Sun: *Powder Metall.*, 2003, vol. 46, pp. 171–74.
22. M. Sarasola, S. Sainz, and F. Castro: *Euro PM 2005*. 2005, pp. 349–56.
23. C. Tojal, T. Gómez-Acebo, and F. Castro: *Mater. Sci. Forum.* 2007, pp. 661–64.
24. M. Skałoń, M. Hebda, K. Sulikowska, and J. Kazior: *Mater. Des.*, 2016, vol. 108, pp. 462–69.
25. M. Momeni, C. Gierl, H. Danninger, I.U. Mohsin, and A. Arvand: *Powder Metall.*, 2012, vol. 55, pp. 212–21.
26. C. Gierl, I.U. Mohsin, and H. Danninger: *Powder Metall. Prog.*, 2008, vol. 8, pp. 135–1.
27. P. Orth, A. Bouvier, and R. Ratzi: *Proc. Euro PM 2004*. 2004, pp. 307–12.
28. R. Oro, M. Campos, C. Gierl-Mayer, H. Danninger, and J.M. Torralba: *Metall. Mater. Trans. A*, 2015, vol. 46, pp. 1349–59.
29. A. Veiga: Development of High Performance Nickel or Boron PM Steels Respectively Obtained after Solid State and Liquid Phase Sintering, PhD thesis, University of Navarra, 2015.
30. J.-O. Andersson, T. Helander, L. Höglund, P. Shi, and B. Sundman: *Calphad*, 2002, vol. 26, pp. 273–312.
31. N.A. Gokcen: *J. Phase Equilibria*, 1991, vol. 12, pp. 313–21.
32. P.K. Liao and K.E. Spear: *ASM Handbook*, ASM International, Ohio, 1991, vol. 3, pp. 2.8–9.8.
33. B. Cao, X. Wang, H. Cui, and X. He: *J. Univ. Sci. Technol. Beijing Miner. Metall. Mater. (Eng Ed)*, 2002, vol. 9, pp. 347–51.
34. W. Wang, S. Zhang, and X. He: *Acta Metall. Mater.*, 1995, vol. 43, pp. 1693–99.
35. M.W. Wu and W.Z. Cai: *MATEC Web Conf.* 2015, p. 1012.
36. J. Liu, A. Cardamone, T. Potter, R.M. German, and F.J. Semel: *Powder Metall.*, 2000, vol. 43, pp. 57–61.
37. M.W. Wu and W.Z. Cai: *Mater. Charact.*, 2016, vol. 113, pp. 90–97.